Received: 5 July 2024 | Revised: 28 August 2024 | Accepted: 27 September 2024

DOI: 10.1002/dug2.70007

RESEARCH ARTICLE

DUSE WILEY

Probability prediction of true-triaxial compressive strength of intact rocks based on the improved PSO-RVM model

Qi Zhang[1] | **Maohui Wang**[1] | **Ning Wang**[1] | **Yixin Shen**[1] | **Xuzhen He**[2]

[1]School of Civil Engineering, Southeast University, Nanjing, China

[2]School of Civil and Environmental Engineering, University of Technology Sydney, Ultimo, Australia

Correspondence

Qi Zhang, School of Civil Engineering, Southeast University, Nanjing 210096, China.
Email: zhangqi@seu.edu.cn

Funding information

China University of Mining and Technology, Grant/Award Number: SKLGDUEK2006; National Natural Science Foundation of China, Grant/Award Numbers: 41602300, 41972277, 42277158

Abstract

In deep underground engineering design, the true-triaxial compressive strength of intact rocks is a critical evaluation index. Traditional methods for acquiring true-triaxial strength data are hampered by labor-intensive manual operations. To mitigate the time-consuming nature of true-triaxial experiments, this study leverages the unique capabilities of the relevance vector machine (RVM) to develop machine learning prediction models. These models aim to streamline the process and enhance predictive accuracy, thereby offering a more efficient alternative to conventional experimental approaches. The proposed models establish a correlation between the major principal stress (σ_1) and the material constants, alongside other Hoek–Brown (H–B) strength parameters. A comprehensive data set, encompassing 408 sets of true-triaxial experimental data from 12 different rock types, was collated from previous studies. This true-triaxial strength data set was systematically divided into three groups based on the intact rock material content (m_i), facilitating subsequent validation efforts. To enhance prediction accuracy and generalization capability, particle swarm optimization (PSO) is employed to optimize the hybrid kernel function parameters of the RVM. This study introduces a dynamic inertia weight decreasing method, demonstrating superior prediction accuracy compared to conventional PSO improvement techniques. In comparison with five three-dimensional H–B type criteria and two other machine learning models, the improved PSO-RVM model demonstrated superior performance across three distinct m_i groups. Additionally, the proposed model is capable of generating probabilistic predictions, thereby effectively capturing the inherent uncertainty associated with rock strength. The probability distribution of model prediction errors closely aligns with that indicated by the generalized Zhang–Zhu criterion, underscoring the improved PSO-RVM model's ability to capture the uncertainty in true-triaxial compressive strength. Furthermore, this study explores sample selection for combined tests integrating true-triaxial experiments and the proposed improved PSO-RVM model, providing a tentative optimal ratio for predicting the true-triaxial compressive strength of intact rocks.

KEYWORDS

intact rock, particle swarm optimization, probabilistic prediction, relevance vector machine, true-triaxial compressive strength

Highlights

- A particle swarm optimization-relevance vector machine (PSO-RVM) model with a hybrid kernel function is developed to predict the major principal stress σ_1.
- A method for improving the PSO algorithm has been proposed.
- The optimal sample ratio for predicting the true triaxial compressive strength of intact rocks has been identified.

1 | INTRODUCTION

Rock strength was one of the important evaluation indexes in deep underground engineering design (Hoek & Brown, 1980b). In recent years, the increased excavation activities in deep rock engineering have frequently encountered phenomena of brittle fracture, such as rock failure and rock bursts, under complex stress paths. These occurrences pose significant threats to the stability of geological engineering projects and the safety of technical personnel (Michelis, 1985, 1987; Mogi, 1966). Accurate prediction of rock strength is crucial for providing technical support in deep underground engineering, as it significantly enhances both the safety and economic efficiency of such projects.

The true triaxial compression test addresses the challenges associated with intermediate principal stress and complex stress paths, which are increasingly critical issues in deep underground engineering. By enabling the independent variation of principal stresses, it accurately reflects the actual loading conditions experienced by rock in situ (Mogi, 1971b). Since Mogi's development of the pioneering intact rock triaxial apparatus (Mogi, 1971a, 1971b, 1972), a variety of true-triaxial apparatuses (TTAs) have been implemented for rock testing. A few TTA adopt flexible loading devices (Smart, 1995), whose three principal stresses are all loaded by the rubber sac. Meanwhile, a triaxial rigid loading device is applied in another type of TTA (Sun et al., 2005; Tiwari & Rao, 2004). The predominant apparatus combines elements from both aforementioned types. In this hybrid TTA configuration, the minor principal stress is induced by a pressure chamber, while the intermediate principal stress is applied through vertically compressible plates (Chang & Haimson, 2000; Feng et al., 2015; Mogi, 1971a). The true-triaxial compression test furnishes essential data for rock mechanics research, model validation, and rock mass stability analysis in the field of deep underground engineering.

The Hoek–Brown (H–B) criterion represents a prevalent model derived from extensive true-triaxial test data on hundreds of rock samples, supported by rigorous statistical analysis (Hoek & Brown, 1980a, 1980b, 1988, 2019). The H–B strength criterion does not account for the influence of the intermediate principal stress, a factor that significantly impacts rock strength in numerous scenarios (Deng et al., 2020; Song et al., 2019; Zhao et al., 2021). In response to this limitation, several three-dimensional strength criteria have been proposed (Pan & Hudson, 1988; Priest, 2005; Single et al., 1998; Zhang & Zhu, 2007; Zhang et al., 2013), aiming to address and mitigate the aforementioned drawbacks.

True-triaxial experiments are hampered by labor-intensive manual operations, posing challenges in obtaining the true-triaxial compressive strength of intact rock using TTA (Babanajad et al., 2017). Moreover, the accuracy of such criteria varies with the geological composition and the complexity of stress combinations (Benz & Schwab, 2008). Furthermore, the inherent uncertainties associated with rock materials, necessitating substantial data for comprehensive characterization, must also be acknowledged (Bozorgzadeh et al., 2018; Contreras et al., 2018; Miranda et al., 2009; Wang & Aladejare, 2016; Xu et al., 2017). To streamline the complexities of true-triaxial experiments and improve predictive accuracy, novel methodologies can be proposed to efficiently and precisely forecast the potential range of rock strength. Recent advancements in machine learning algorithms have shown rapid development in predictive research, owing to their broad applicability and robust performance. Moreover, these methods often yield highly reliable and accurate outcomes, circumventing the need for a predefined structure in addressing critical issues (Liu et al., 2015; Zhang et al., 2019).

Various machine learning methodologies have been investigated to develop diverse prediction models. For instance, artificial neural networks (ANN) (Azoor et al., 2022; Yu et al., 2021) and support vector machines (SVM) (Li & Tan, 2016; Miah et al., 2020; Ren et al., 2018) are prevalent algorithms that have demonstrated successful applications in prediction tasks. Intelligent algorithms often struggle to produce consistent probability outputs and fail to deliver probabilistic prediction results reliably. Additionally, unoptimized traditional algorithms may exhibit drawbacks such as overfitting and local optimization, influenced by data set noise and the principles of structural risk minimization. The relevance vector machine (RVM) stands out as a robust regression method grounded in the Bayesian framework (Tipping, 1999, 2000). RVM, akin to SVM, circumvents constraints associated with the necessity for a positive-definite kernel (Karimi & McAuley, 2016), distinguishing itself in its approach to regression tasks. Moreover, the relevance vectors in RVM exhibit greater sparsity compared to the support vectors in SVM, thereby enhancing computational efficiency during testing (Ceryan, 2014). To refine the kernel function parameters within RVM, particle swarm optimization (PSO) (Kennedy & Eberhart, 1995) is employed. PSO, recognized as a stochastic optimization technique, has found extensive application in optimizing model parameters in rock engineering studies (Babanouri et al., 2013; Jahed Armaghani et al., 2015; Shinoda & Miyata, 2019).

This study introduces an optimized RVM model using an improved PSO algorithm to predict the true-triaxial compressive strength of intact rocks based on the H–B strength criterion. A comprehensive true-triaxial database comprising 408 datasets sourced from the literature forms the basis for establishing the PSO-RVM model, which is subsequently validated. Considering the distinct properties of intact rock materials, the data set is stratified into three distinct groups. Following iterative optimization using the PSO algorithm, the PSO-RVM model was constructed. Validation of the predictive accuracy of this model involved comparative analyses with two other machine learning approaches. An improved method for the PSO algorithm was introduced, demonstrating superior performance over traditional PSO improvement techniques. The predictive capabilities of the improved model were assessed using true-triaxial experimental data and validated against five three-dimensional H–B criteria through various statistical metrics. Additionally, the paper discusses the selection of samples for combined tests based on true-triaxial experiments and the proposed improved PSO-RVM model.

2 | METHODOLOGY AND APPLICATION OF THE PSO-RVM MODEL

2.1 | Methodology

2.1.1 | Relevance vector machine

RVM represents a Bayesian sparse kernel method used in both regression and classification problems (Tipping, 2000). This approach effectively bypasses the primary constraints associated with SVM, particularly the requirement for positive definiteness in kernel functions. Given a data set denoted as the training sample set $\{x_i, t_i\}_{i=1}^N$, where N signifies the total number of samples, $\{x_i\}_{i=1}^N$ denotes the input vector, and $\{t_i\}_{i=1}^N$ represents the corresponding target vector. Simultaneously, the target vector can be expressed as the sum of the model output $y(x;\omega)$, depicted in Equation (1).

$$t_i = y(x;\boldsymbol{\omega}) + \varepsilon_i, \tag{1}$$

where ε_i is the Gaussian noise element with zero mean and variance σ^2, which is denoted by $\varepsilon_i \in N(0, \sigma^2)$.

The regression function $y(x;\omega)$ for the target values is defined by

$$y(x;\boldsymbol{\omega}) = \sum_{i=1}^{N} \omega_i K(x, x_i) + \omega_0, \tag{2}$$

where $K(x, x_i)$ represents the kernel function; $\boldsymbol{\omega} = [\omega_0, \omega_1, \ldots, \omega_N]^{\mathrm{T}}$ denotes the weighted parameter vector corresponding to the kernel function.

$p(t_i|x)$ follows the normal distribution N. Its distribution is expressed as

$$p(t_i|x) = N[t_i|y(x_i;\boldsymbol{\omega}), \sigma^2]. \tag{3}$$

Assuming that $\{t_i\}_{i=1}^N$ is independent, thus the probability distribution of t is determined by

$$\begin{aligned} p(t|\boldsymbol{\omega}, \sigma^2) &= \prod_{i=1}^{N} N[t_i|y(x_i;\boldsymbol{\omega}), \sigma^2] \\ &= (2\pi\sigma^2)^{-N/2} \exp\left(-\frac{\|t - \boldsymbol{\Phi}\boldsymbol{\omega}\|^2}{2\sigma^2}\right). \end{aligned} \tag{4}$$

where $\boldsymbol{\Phi}$ is a designed matrix of the kernel function and is expressed as

$$\boldsymbol{\Phi} = \begin{bmatrix} 1 & K(x_1, x_1) & \cdots & K(x_1, x_N) \\ 1 & K(x_2, x_1) & \cdots & K(x_2, x_N) \\ \vdots & \vdots & \ddots & \vdots \\ 1 & K(x_N, x_1) & \cdots & K(x_N, x_N) \end{bmatrix}, \tag{5}$$

When a new target vector t^* is given, the probability distribution can be derived by

$$p(t^*|t) = \int p(t^*|\boldsymbol{\omega}, \sigma^2) \frac{p(t|\boldsymbol{\omega}, \sigma^2) p(\boldsymbol{\omega}, \sigma^2)}{p(t)} \mathrm{d}\omega \mathrm{d}\sigma^2. \tag{6}$$

In addressing the challenge of overfitting arising from maximum likelihood estimation of the weight vector and variance, a constraint superposition technique is applied, utilizing Bayes' theorem. A prior distribution, described by a zero-mean constraint over the weight vector as outlined in Equation (7), is introduced for this purpose.

$$p(\omega_i|\alpha_i) = N(\omega_i|0, \alpha_i^{-1}), \tag{7}$$

where $\boldsymbol{\alpha} = [\alpha_0, \alpha_1, \ldots, \alpha_N]$ represents the hyper-parameter vector, which controls the amount of the weights deviated from zero.

The posterior distribution over the weights is expressed by

$$\begin{aligned} &p(w \mid t, \boldsymbol{\alpha}, \sigma^2) \\ &= (2\pi)^{-N/2} \left|\sum\right|^{-1/2} \exp\left[-\frac{1}{2}(\boldsymbol{\omega} - \mu)^T \sum^{-1} (w - \mu)\right], \end{aligned} \tag{8}$$

where $\boldsymbol{\Sigma}$ represents a posterior covariance matrix, which is denoted by $\Sigma = (\sigma^{-2}\boldsymbol{\Phi}^T\boldsymbol{\Phi} + A)^{-1}$; A =diag $(\alpha_0, \alpha_1, \ldots, \alpha_N)$; $\mu = \sigma^{-2}\sum\boldsymbol{\Phi}^T t$.

$$(\alpha_{\mathrm{MP}}, \sigma^2_{\mathrm{MP}}) = \arg\max_{\alpha,\sigma^2} p(t|\alpha, \sigma^2). \tag{9}$$

Since the values of α_{MP} and σ^2_{MP} cannot be calculated directly, an iterative estimation approach is employed, which is summarized as

$$\alpha_i^{\mathrm{new}} = \frac{1 - \alpha_i \Sigma_{ii}}{\mu_i^2}, \tag{10}$$

$$(\sigma^2)^{\mathrm{new}} = \frac{\|t - \boldsymbol{\Phi}\mu\|^2}{N - \sum_{i=0}^{N}(1 - \alpha_i \Sigma_{ii})}, \tag{11}$$

where Σ_{ii} is the i-th diagonal element of Σ.

Based on the given approximate values of α and σ^2, the approximations of α_{MP} and σ^2_{MP} are obtained by updating Equations (10) and (11).

2.1.2 | Particle swarm optimization

PSO is recognized as a straightforward yet effective optimization technique. Within an n-dimensional search space, a fixed number of particles, determined by the algorithm's configuration, explore potential permutations. Each particle encapsulates a specific permutation and assesses its fitness based on current position evaluations (Eberhart & Shi, 1998). The model's search space is repeatedly traversed by the particles. The particles within the model continuously explore the search space, influenced by their individual current positions and optimal positions, as well as those of other particles (Poli et al., 2007). Each particle gradually traverses

the search space and exchanges information with other particles. The updating rules for velocity and position are specified in Equations (12) and (13), respectively.

$$v_i^{k+1} = \beta v_i^k + M_1(p_i^k - x_i^k) + M_2(g_i^k - x_i^k), \quad (12)$$

$$x_i^{k+1} = x_i^k + v_i^{k+1}, \quad (13)$$

where k represents the iteration number; v_i represents the velocity; x_i is the position of each particle; p and g are the best place of the singular molecule and the best situation among all particles in the multitude, separately; and M_1 and M_2 are hyper-boundaries inside the reach [0, 4]. β is a dormancy factor from 0.4 to 0.9 to control the verifiable change in speed for the ongoing effect.

2.1.3 | Kernel function and hyperparameters

To mitigate the computational challenges posed by high-dimensional feature spaces, kernel functions often utilize inner product operations as an efficient alternative to more complex computations. This approach dictates how samples are mapped from lower-dimensional to higher-dimensional spaces based on the selected kernel function type. Moreover, the parameters chosen for the kernel function critically influence the predictive performance of machine learning models.

The prevalent kernel functions in use include the following: (1) Local kernels, such as Gaussian kernels, known for their robust local interpolation capabilities and (2) global kernels, such as polynomial kernels, recognized for their strong generalization capabilities (Ma et al., 2020). Considering the characteristics of intact rocks, the primary principal stress is influenced by multiple factors, with minor variations in each factor potentially resulting in significant changes in magnitude. Therefore, the model requires specific local interpolation capabilities. At the same time, the wide range of values associated with each factor highlights the need for the model to possess sufficient generalization capabilities. To integrate the advantageous features of both local interpolation and generalization into the kernel function, a hybrid kernel function is proposed as defined by

$$K(x, x_i) = \theta \exp(-\|x - x_i\|^2/c^2) + (1 - \theta)(xx_i + 1)^q, \quad (14)$$

where c is the Gaussian kernel parameter (bandwidth parameter); q is the polynomial kernel parameter; and θ is the proportional parameter of the hybrid kernel function.

Given its notable capabilities, the Gaussian-polynomial hybrid kernel function is incorporated into the proposed PSO-RVM model. This hybrid kernel function incorporates three parameters: θ, c, and q. While the specific values of these parameters are not explicitly defined, they are closely linked to the model's predictive accuracy. The PSO algorithm is utilized to optimize these parameters within the hybrid kernel function framework, thereby establishing a strength prediction model based on PSO-RVM using the hybrid kernel.

2.2 | Input parameters selection

The prediction of true-triaxial compressive strength in intact rocks essentially entails forecasting the major principal stress. Input parameters are selected in accordance with the H–B strength criterion, which has been extensively validated across a diverse array of true-triaxial experiments and remains a cornerstone in geotechnical engineering (Hoek & Brown, 1980a, 1980b, 2019). The mathematical expression for the H–B criterion is expressed by

$$\sigma_1 = \sigma_3 + \sigma_c \sqrt{m_i \frac{\sigma_3}{\sigma_c} + 1}, \quad (15)$$

where σ_1 and σ_3 are the major and minor principal stresses, respectively; σ_c is the unconfined compressive strength; and m_i is the material constant for the intact rock.

Thus, the compiled data set comprises five variables: intermediate principal stress σ_2, minor principal stress σ_3, unconfined compression strength σ_c, and material constant m_i as input parameters, with major principal stress σ_1 designated as the model output.

2.3 | Data set preparation and *k*-fold cross-validation

The models were developed using data derived from 408 true-triaxial experiments compiled from various previous studies (Chang & Haimson, 2000; Gao et al., 2018; Haimson & Chang, 2000; Mogi, 1971b; Takahashi & Koide, 1989; Wang & Kemeny, 1995; Xu et al., 2017; Zhao et al., 2018). This data set encompasses 12 distinct rock types and spans a wide range of major principal stresses, significantly enhancing the robustness of the proposed models.

To assess the model's predictive performance across various rock types, the data set is stratified into three groups based on the material constant m_i range. Each group comprises over 100 data points encompassing at least three distinct rock types. Detailed specifics of each prediction group are outlined in Table 1.

To derive more insightful insights from the limited data sets, this study employed k-fold cross-validation, with k set to 5. For each prediction group, 30 data points were randomly allocated to form the test set, while the remaining data comprised the training set. The training set for each group is divided into five equal parts. In each iteration, the model is trained on four parts, while the remaining part is used to evaluate the model's accuracy. This process is repeated five times, with a different subset used for validation in each round. The model's optimal parameters are determined based on the highest average accuracy across these five training sessions.

2.4 | Data normalization and model performance evaluation method

To reduce the model accuracy loss and accelerate the algorithm learning speed, the input and output data are

TABLE 1 Data amount and rock types in each prediction group.

Group label	Range of m_i	Group data amount	Rock type	m_i	Sample amount	Source
#m_i-low	$0 < m_i \leq 15$	143	Yuubari shale	6	26	Takahashi and Koide (1989)
			Dunham dolomite	10	53	Mogi (1971b)
			Mizuho trachyte	11	31	Mogi (1971b)
			Jinping marble A	11	20	Zhao et al. (2018)
			Jinping marble B	13	13	Gao et al. (2018)
#m_i-medium	$15 < m_i \leq 25$	119	Shirahama sandstone	16	43	Takahashi and Koide (1989)
			Apache leap tuff	17	49	Wang and Kemeny (1995)
			Pakistan sandstone	19	27	Gao et al. (2018)
#m_i-high	$m_i > 25$	146	Linhai granite	29	51	Xu et al. (2017)
			KTB amphibolite	29	40	Chang and Haimson (2000)
			Beishan granite	30	10	Gao et al. (2018)
			Westerly granite	32	45	Haimson and Chang (2000)

normalized using min–max normalization. All data are normalized to the range of 0–1 by

$$z_i' = \frac{z_i - z_{\min}}{z_{\max} - z_{\min}}, \tag{16}$$

where z_i' is the data after normalization; z_i is the original data; and $z_{\max}$ and $z_{\min}$ are the maximum and minimum values of the original data, respectively. Different predictions may have different parameter requirements. Therefore, the optimization of the model structure is essential to minimize the uncertainty of model misspecifications.

To comprehensively evaluate the prediction model performance, several statistical indices are applied including coefficient of determination (R^2), mean absolute percentage error ($MAPE$), mean absolute error (MAE), and root mean square error ($RMSE$). The mathematical expressions of the above statistical index are expressed by

$$R^2 = \frac{\sum_{i=1}^{n}(\sigma_{1,\text{ob-}i} - \sigma_{\text{mean}})^2 - \sum_{i=1}^{n}(\sigma_{1,\text{ob-}i} - \sigma_{1,\text{pr-}i})^2}{\sum_{i=1}^{n}(\sigma_{1,\text{ob-}i} - \sigma_{\text{mean}})^2}, \tag{17}$$

$$MAPE = \frac{100\%}{n}\sum_{i=1}^{n}\left|\frac{\sigma_{1,\text{pr-}i} - \sigma_{1,\text{ob-}i}}{\sigma_{1,\text{ob-}i}}\right|, \tag{18}$$

$$MAE = \frac{1}{n}\sum_{i=1}^{n}\left|\sigma_{1,\text{ob-}i} - \sigma_{1,\text{pr-}i}\right|, \tag{19}$$

$$RMSE = \sqrt{\frac{1}{n}\sum_{i=1}^{n}(\sigma_{1,\text{ob-}i} - \sigma_{1,\text{pr-}i})^2}, \tag{20}$$

where $\sigma_{1,\text{ob}-i}$ and $\sigma_{1,\text{pr}-i}$ represent the observed and predicted major principal stress data, respectively. σ_{mean} is the mean of the observed values, and n is the number of the sample in the data set under consideration. Theoretically, for an excellent statistical model, the R^2 is 100%, while MAE, $MAPE$, and $RMSE$ are 0 (Yagiz et al., 2012).

2.5 | Application of the PSO-RVM model

The RVM model serves as the primary approach for predicting the major principal stress, with the PSO algorithm utilized to optimize kernel function parameters for RVM. The algorithmic flowchart depicting the proposed improved PSO-RVM model is illustrated in Figure 1. An extensive data set comprising a significant volume of experimental true-triaxial data is compiled, and the primary variables for the RVM model are organized according to the H–B criterion. All data undergo normalization, and subsequently, the data set is stratified into three groups encompassing both training and testing sets based on the material constant m_i of the rock specimens. Following iterative optimization and model training phases, the PSO algorithm identified optimal kernel function parameters for constructing the PSO-RVM model. Comparative analysis with two alternative machine learning models validated the superior predictive accuracy of the PSO-RVM approach. Furthermore, an improved PSO algorithmic method was introduced. Finally, the improved model's performance was validated against five three-dimensional H–B type criteria to assess its efficacy.

3 | VALIDATION OF THE PSO-RVM MODEL

3.1 | Validation of the PSO-RVM model based on data sets

Utilizing the three data set groups, the PSO algorithm was employed to optimize kernel function parameters for the RVM model. In this study's PSO algorithm, the particle count was configured to 60, with 100 iterations

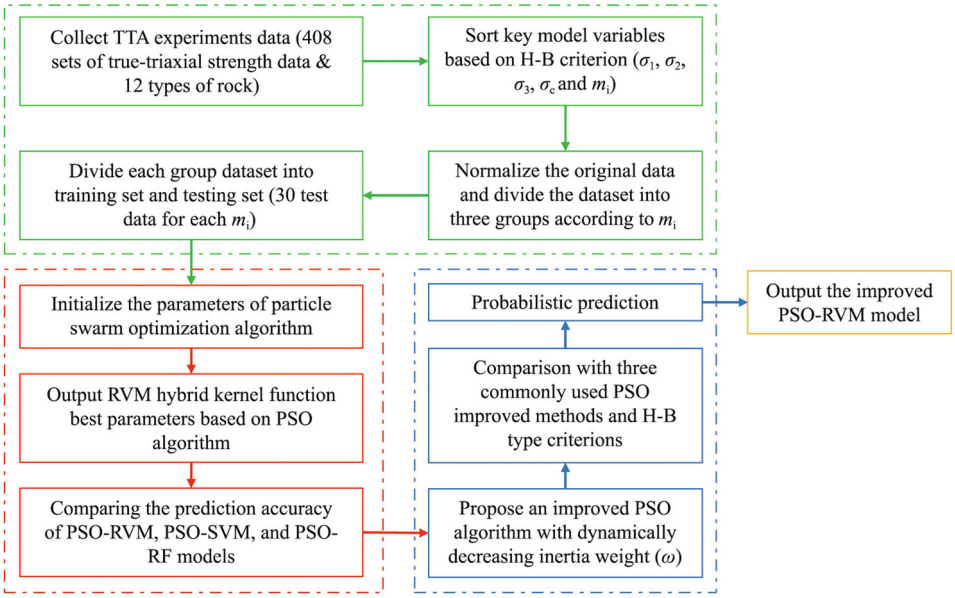

FIGURE 1 Flowchart of the proposed model for probabilistic prediction of true-triaxial compressive strength.

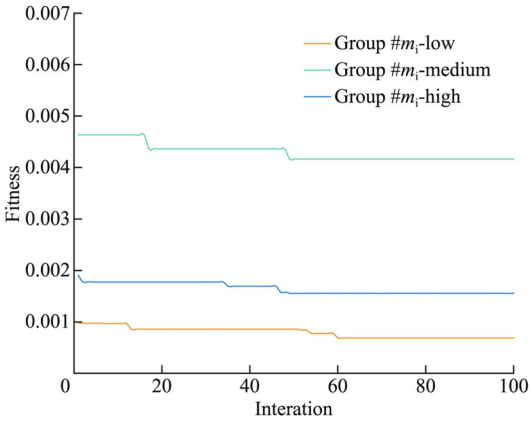

FIGURE 2 Relationship of fitness and iterations during particle swarm optimization (PSO) operation.

performed, and initial parameters β, M_1, and M_2 set to 0.8, 1.6, and 1.2, respectively. Upon achieving the minimum *RMSE*, the optimal kernel function parameters for the *RVM* model are conclusively identified. The relationship between fitness and iterations during PSO operation is visually depicted in Figure 2. The figure illustrates that fitness stabilizes as the number of iterations increases. Variations in the final fitness among the three groups are attributed to differences in the quantity and characteristics of the rocks within each group. Table 2 presents the optimized kernel function parameters. The parameter θ ranges from 0.20 to 0.50, c ranges from 0.30 to 1.00, and q ranges from 1.00 to 2.50. These parameter values are crucial for developing future models under uncertain conditions.

Figure 3 illustrates the prediction results of the PSO-RVM model for three groups based on the testing set. The prediction error of σ_1 is represented by the distance from each data point to the 1:1 diagonal line. The results indicate that the predicted values in the testing sets

TABLE 2 Optimized parameters of the kernel function.

Group	θ	c	q
#m_i-low	0.473	0.601	1.849
#m_i-medium	0.477	0.426	2.367
#m_i-high	0.239	0.497	2.288

closely align with the diagonal line. Across the three data set groups, the R^2 values are 0.978, 0.914, and 0.940, with corresponding *RMSE* values of 29.736, 23.127, and 67.610, respectively. These results demonstrate that all three models effectively predict the major principal stress σ_1, exhibiting high R^2 and low *RMSE* values. They notably capture the intricate relationship between input and output parameters.

3.2 | Testing set result comparison between machine learning models

To assess the efficacy of RVM relative to other intelligent algorithms, support vector machine (SVM) and random forest (RF) algorithms were incorporated into the prediction process. SVM and RF are widely recognized for their robust generalization capabilities in machine learning. The PSO algorithm was employed to optimize parameters for both SVM and RF models. Specifically, for SVM, a radial basis function was utilized, and PSO was applied to determine optimal values for the penalty coefficient (c_p) and loss coefficient (c_l). For RF, the PSO algorithm was employed to optimize the number of decision trees. The data set to train and test the machine learning models is identical to RVM, which includes three divided groups of training set and testing set. Table 3 presents the optimized parameters of SVM and RF.

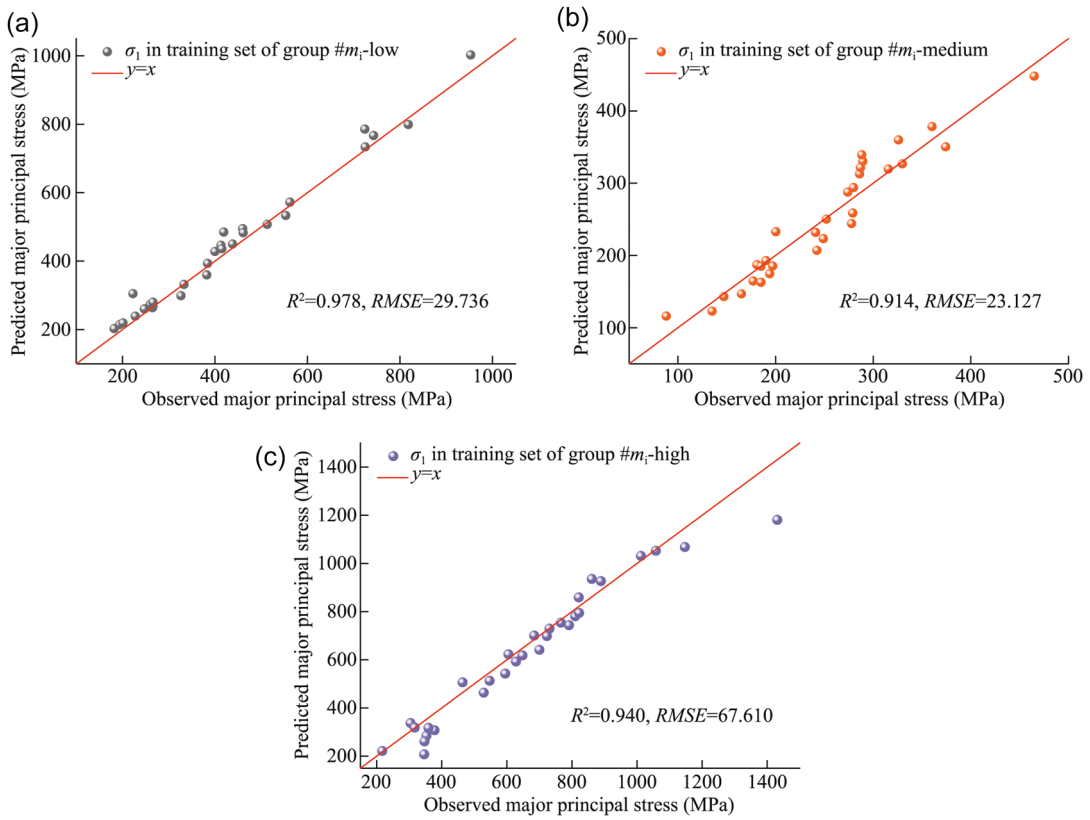

FIGURE 3 PSO-RVM model prediction results of three groups in the testing set. (a) Group #m_i-low; (b) Group #m_i-medium; and (c) Group #m_i-high.

TABLE 3 Optimized parameters of SVM and RF.

Group	SVM		RF
	c_p	c_1	Trees
#m_i-low	191.475	0.0306	22
#m_i-medium	187.442	0.0526	23
#m_i-high	10.627	0.0067	45

The comparison of prediction results between PSO-RVM, PSO-SVM, and PSO-RF models is shown in Figure 4. As illustrated in Figure 4, the PSO-RVM model demonstrates the highest prediction accuracy across all three groups. These findings underscore the PSO-RVM model's superiority over the other two machine learning models.

4 | IMPROVED PSO ALGORITHM APPLIED TO THE MODEL AND PROBABILITY PREDICTION

4.1 | Improvement of the PSO algorithm

The inertia weight (β) serves as a crucial parameter in the PSO algorithm, determining a particle's ability to maintain its previous velocity. Higher values of inertia weight facilitate global search, whereas lower values promote local search. Hence, exploring enhancements to the PSO algorithm by investigating inertia weights holds substantial significance. To achieve an optimal balance between global and local search capabilities, this study introduces a novel approach for dynamically updating the inertia weight (β):

Improved method (a): The initial inertia weight is initialized at 0.9, gradually decreasing to a final value of 0.4. To mitigate the risk of converging to local optima, it is essential to maintain a relatively high inertia weight (β) during the early stages of optimization. As the optimization process advances, prioritizing local search becomes increasingly crucial to achieve more precise search outcomes. To operationalize this approach, Equation (21) introduces a cubic decreasing function for the inertia weight (β), dynamically adjusting it based on the number of iterations.

$$\beta = \beta_{\max} - (\beta_{\max} - \beta_{\min}) \times \left[2.5\frac{i}{T} - 2.2\left(\frac{i}{T}\right)^2 + 0.7\left(\frac{i}{T}\right)^3\right], \quad (21)$$

where i represents the number of iterations and T represents the maximum number of iterations.

To validate the advantages of improved method (a), it was compared with three commonly used dynamic adjustment methods for inertia weight. Similar to method (a), the initial inertia weight for these three methods was set to 0.9 and eventually reduced to 0.4.

Improved method (b): The inertia weight decreases in a linear fashion (Shi & Eberhart, 1999) as defined by

$$\beta = \beta_{\max} - \frac{i}{T}(\beta_{\max} - w_{\min}). \quad (22)$$

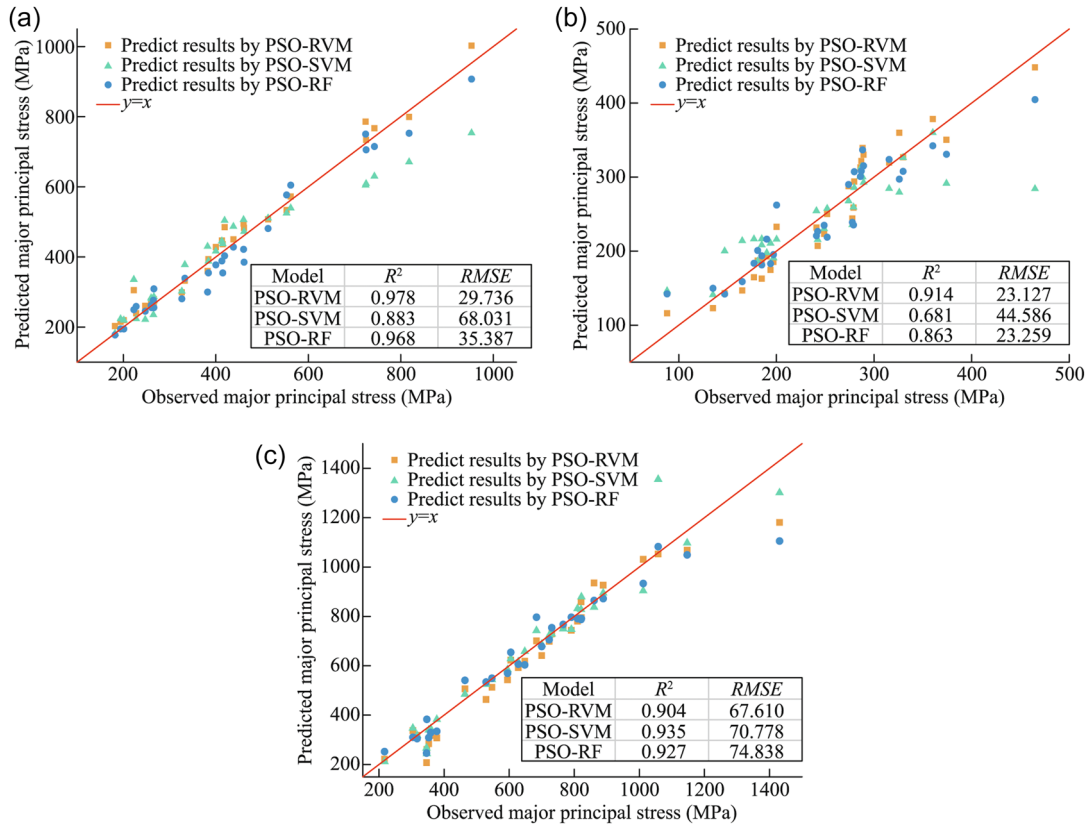

FIGURE 4 Comparison of prediction results between PSO-RVM, PSO-SVM, and PSO-RF models. (a) Group #m_i-low; (b) Group #m_i-medium; and (c) Group #m_i-high.

Improved method (c): The inertia weight decreases following a quadratic function form as defined by

$$\beta = \beta_{max} - (\beta_{max} - \beta_{min}) \times \left[\frac{2i}{T} - \left(\frac{i}{T}\right)^2\right]. \quad (23)$$

Improved method (d): The inertia weight decreases according to an alternative quadratic function form (Yang et al., 2015) as defined by

$$\beta = \beta_{max} - (\beta_{max} - \beta_{min}) \times \left(\frac{i}{T}\right)^2. \quad (24)$$

4.2 | Comparison of the improved PSO-RVM results

On the Group #m_i-low data set, all four improvement methods yielded significant results. However, on the datasets of Group #m_i-medium and Group #m_i-high, the prediction accuracy of improvement methods (b) and (c) did not surpass that of the original PSO algorithm. As illustrated in Figure 5, the improved method (a) proposed in this study achieved the highest prediction accuracy across all three groups. Furthermore, a comparison of the computation times for each method revealed that method (a) had the shortest computation time. Therefore, it is justified to optimize the PSO algorithm using improved method (a).

4.3 | Testing set results comparison between empirical criteria

Research on the mechanical response of rocks under true-triaxial stress combinations has been extensively investigated (Pan & Hudson, 1988; Priest, 2005; Single et al., 1998; Zhang, 2008; Zhang & Zhu, 2007). Utilizing data derived from true-triaxial experiments, this study proposes a set of three-dimensional H–B type rock strength criteria, which are succinctly summarized in Table 4.

To further verify the predictive accuracy of the improved PSO-RVM model for major principal stress, its predictions are juxtaposed against established criteria including the Generalized Pan–Hudson criterion (GPH), Generalized Singh criterion (GS), Generalized Priest criterion (GP), Simplified Priest criterion (SP), and Generalized Zhang–Zhu criterion (GZZ). The predicted outcomes using H–B type criteria and the improved PSO-RVM model are presented in Table 5. Statistical metrics including *MAPE*, *MAE*, and *RMSE* are utilized as evaluative indices for prediction accuracy. The mean *MAPE* value for the proposed improved PSO-RVM model across three groups is notably low at 6.262%, demonstrating a significant improvement compared to the GPH, GS, GP, and SP criteria and marginally better than the GZZ criterion. With the exception of the GZZ criterion, the performance of the remaining criteria is markedly inferior to that of the proposed model. These findings conclusively highlight the superior predictive

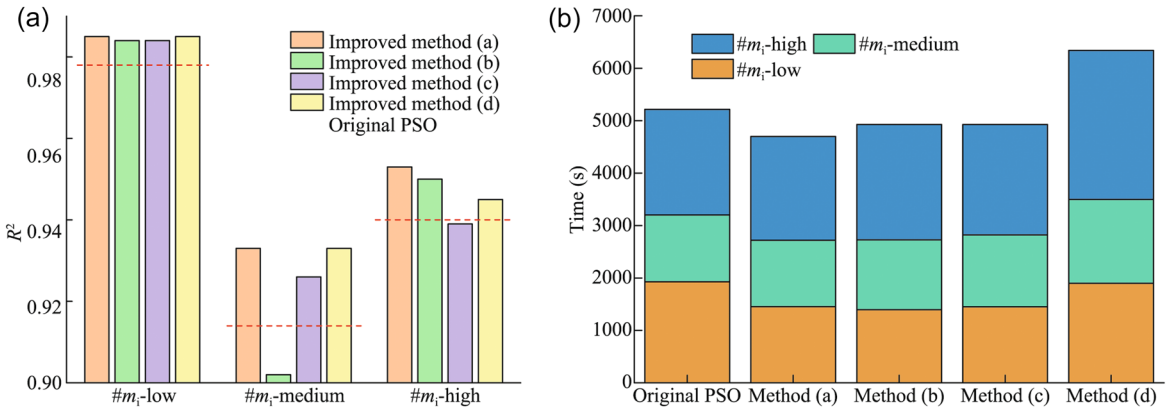

FIGURE 5 Comparison of the prediction results of four different improved PSO-RVM models. (a) Prediction accuracy, (b) computation time.

TABLE 4 Hoek–Brown (H–B)-type strength criteria.

Strength criterion	Expression formula
Generalized Pan–Hudson criterion (GPH) (Pan & Hudson, 1988)	$s\sigma_c = \frac{1}{\sigma_c^{1/a-1}}\left(\frac{3\tau_{oct}}{\sqrt{2}}\right)^{1/a} + \frac{3m_b\tau_{oct}}{2\sqrt{2}} - m_b\frac{I_1}{3}$
	$\tau_{oct} = \frac{1}{3}\sqrt{(\sigma_1-\sigma_2)^2+(\sigma_2-\sigma_3)^2+(\sigma_3-\sigma_1)^2}$
	$I_1 = \sigma_1+\sigma_2+\sigma_3$
Singh criterion (Singh) (Single et al., 1998)	$\sigma_1 = \sigma_3 + \sigma_c\left[\frac{m_b(\sigma_2+\sigma_3)}{2\sigma_c} + s\right]^a$
Generalized Priest criterion (GP) (Priest, 2005)	$\sigma_1 = 3\sigma_{3hb} + \sigma_c\left[\left(\frac{m_b\sigma_{3hb}}{\sigma_c}\right) + s\right]^a - (\sigma_2+\sigma_3)$
	$\sigma_{3hb} = \frac{\sigma_2+\sigma_3}{2} + \frac{-E \pm \sqrt{E^2 - F(\sigma_2-\sigma_3)^2}}{2F}$
	$E = 2C^a\sigma_c,\ F = 3 + 2aC^{a-1}m_b,\ C = s + \frac{m_b(\sigma_2+\sigma_3)}{2\sigma_c}$
Simplified Priest criterion (SP) (Priest, 2005)	$\sigma_1 = 3\sigma_{3hb} + \sigma_c\left[\left(\frac{m_b\sigma_{3hb}}{\sigma_c}\right) + s\right]^a - (\sigma_2+\sigma_3)$
	$\sigma_{3hb} = \omega\sigma_2 + (1-\omega)\sigma_3,\ \omega = \alpha\sigma_3^{\beta},\ \alpha = \beta = 0.15$
Generalized Zhang–Zhu criterion (GZZ) (Zhang & Zhu, 2007)	$s\sigma_c = \frac{1}{\sigma_c^{1/a-1}}\left(\frac{3\tau_{oct}}{\sqrt{2}}\right)^{1/a} + \frac{3m_b\tau_{oct}}{2\sqrt{2}} - m_b\frac{\sigma_1+\sigma_3}{2}$

a and s represent rock material constants; I_1 represents first stress invariant; σ_{3hb} represents assumed stress in Priest strength criterion; τ_{oct} represents octahedral shear stress.

accuracy of the improved PSO-RVM model over the three-dimensional H–B type criteria.

Due to inherent rock variability and experimental uncertainties, prediction errors are inevitable. These discrepancies between criterion-predicted outcomes and observed values illustrate such uncertainties. The probability density function (PDF) depicting the prediction errors across three testing sets is presented in Figure 6. The prediction error quantifies the discrepancy between predicted and actual values. Across all three testing sets, it is evident that the improved PSO-RVM model exhibits a mean prediction error close to zero. Furthermore, the variance of its predictions is comparatively lower than that of other models, indicating a closer alignment with true-triaxial experimental data. The error distribution observed in the improved PSO-RVM model closely resembles that of the GZZ criterion, which exhibits superior prediction accuracy among the five criteria evaluated. This similarity underscores the improved PSO-RVM model's robust capability in characterizing uncertainty associated with true-triaxial compressive strength prediction.

4.4 | Probability prediction of the improved PSO-RVM model

By integrating optimized kernel function parameters with model training on the training sets, the improved PSO-RVM model has been successfully developed. The output parameter, major principal stress σ_1, is hypothesized to follow a Gaussian distribution. The model's probability

TABLE 5 Comparison of the prediction results between empirical criteria and the improved PSO-RVM model.

Group	Index	GPH	Singh	GP	SP	GZZ	PSO-RVM
#m_i-low	*MAPE* (%)	21.723	6.666	11.093	7.702	3.686	4.276
	MAE	98.539	30.691	56.097	38.763	17.049	16.630
	RMSE	109.615	42.091	74.399	48.014	21.108	24.176
#m_i-medium	*MAPE* (%)	35.739	15.313	19.494	16.837	9.027	7.108
	MAE	98.704	42.977	54.442	46.499	25.940	16.582
	RMSE	112.941	75.047	89.605	74.690	42.465	20.423
#m_i-high	*MAPE* (%)	32.258	24.630	30.301	15.883	7.619	7.403
	MAE	221.916	136.423	173.977	81.001	48.383	41.310
	RMSE	252.195	202.763	247.937	111.780	59.663	59.756
Mean value	*MAPE* (%)	29.907	15.536	20.296	13.474	6.777	6.262
	MAE	139.720	70.030	94.839	55.421	30.457	24.841
	RMSE	158.250	106.634	137.314	78.161	41.079	34.785

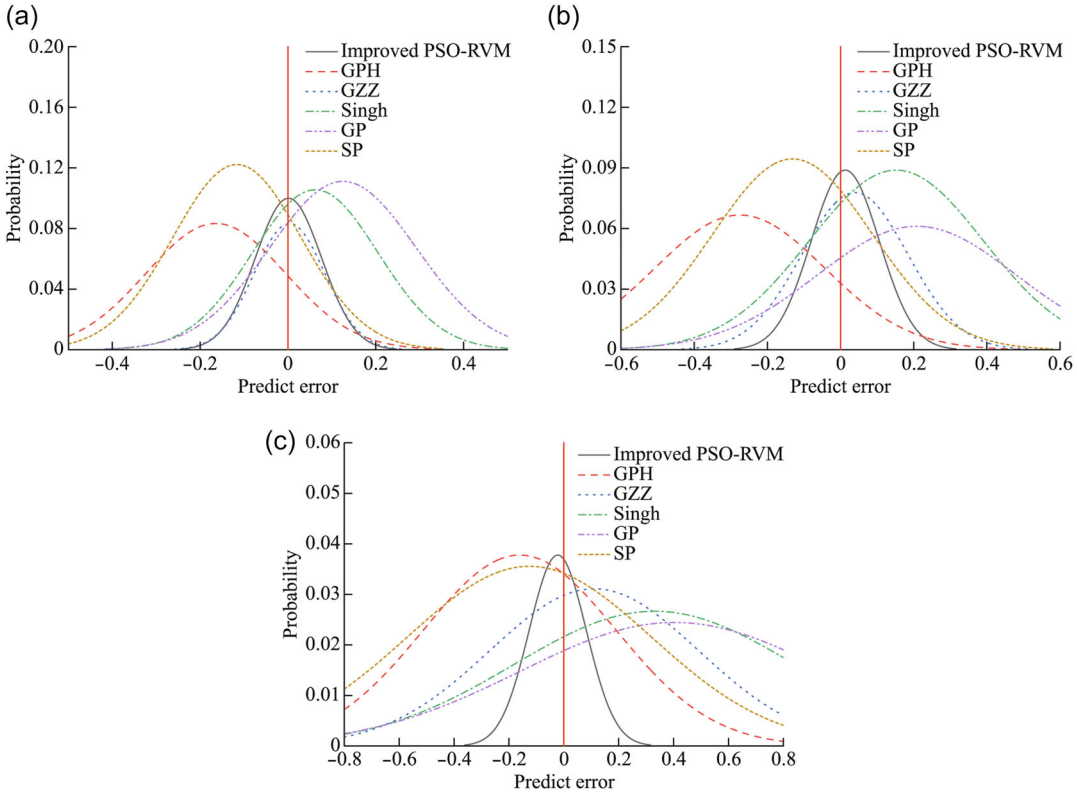

FIGURE 6 Improved PSO-RVM model prediction error of the three groups in the testing set. (a) Group #m_i-low, (b) Group #m_i-medium, and (c) Group #m_i-high.

prediction is subsequently verified using the testing set results. Utilizing the mean and variance of the model's prediction results, the upper and lower bounds of the 95% confidence interval were determined for the improved PSO-RVM model. Figure 7 presents the prediction results of the improved PSO-RVM model for the three groups within the testing set. In Figure 7, the red stars represent the predicted mean values, while the yellow triangles denote the actual values. The blue shaded area indicates the 95% confidence interval for the prediction results. The minor discrepancy between the predicted mean values and the actual values, with the actual values largely falling within the 95% confidence interval, suggests that the prediction results are both stable and reliable. For various rock types, the prediction error of the improved PSO-RVM model exhibits minimal fluctuation, indicating that the model's prediction accuracy is largely unaffected by rock type. Nonetheless, several

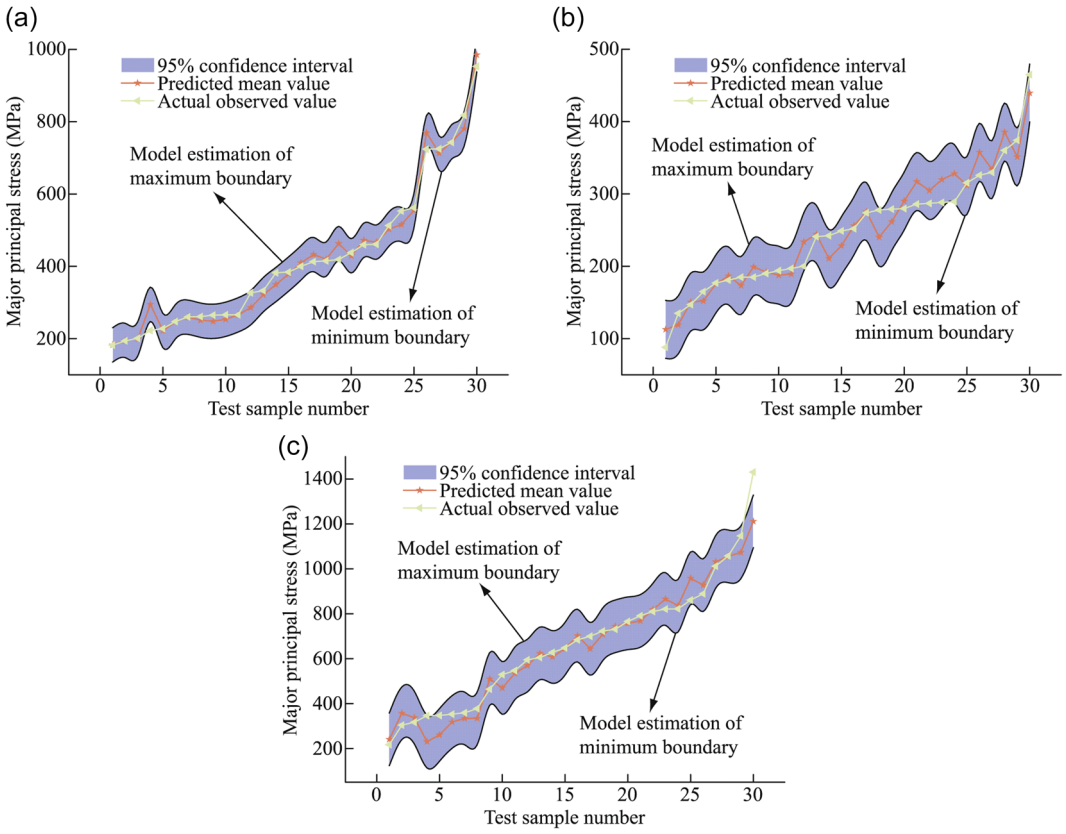

FIGURE 7 Improved PSO-RVM model probability prediction results of the three groups in the testing set. (a) Group #m_i-low, (b) Group #m_i-medium, and (c) Group #m_i-high.

prediction points in Group #m_i-low slightly deviate from the predicted confidence interval. The predicted results from the H–B type criteria also exhibit fluctuations. This deviation may stem from the inherent uncertainty of the rock or errors during the experimental process. Consequently, given sufficient data, the trained model can be effectively utilized to predict the behavior of various rock types.

5 | DISCUSSION ON SAMPLE SELECTION FOR COMBINED TESTS BASED ON TTA EXPERIMENTS AND THE IMPROVED PSO-RVM MODEL

Statistical analysis of the aforementioned rock strength data reveals that the proposed improved PSO-RVM model demonstrates high predictive accuracy and robust performance compared to both three-dimensional H–B type criteria and other machine learning models. For accurate characterization of a rock material's stress response under true-triaxial conditions, it is essential to conduct true-triaxial experiments. As shown in Table 1, characterizing the triaxial properties of rocks, particularly those with a high m_i value, typically necessitates a substantial data set, averaging approximately 40 data sets. Acquiring sufficient true-triaxial data through numerous experiments is time-consuming. Therefore, it is crucial to develop methods that reduce the number of required TTA experiments while effectively increasing the data volume. The ratio of true-triaxial experimental data to data generated by the improved PSO-RVM model is crucial, as it influences the credibility of the experimental findings. The improved PSO-RVM model can reliably generate substantial amounts of data. Consequently, the model is employed to explore sample selection in combined test scenarios.

In the subsequent testing phase, the data set is partitioned into training and testing sets according to a specified proportion. For instance, KTB Amphibolite (Chang & Haimson, 2000) features 40 rock data sets with a uniaxial compressive strength of 165 MPa and a m_i range of 27–32. The parameter settings for the improved PSO-RVM model align with those of the prediction model for the group #m_i-high. The detailed implementation process is outlined as follows:

1. The original data of KTB Amphibolite were normalized using min–max normalization. The parameter settings for the improved PSO-RVM model were determined based on the material constant m_i.
2. The data set was partitioned into training and testing sets using various ratios, ranging from 1:3 to 4:1. Specifically, the partition ratios used were 0.33:1.00, 0.6:1.00, 1:1, 1.22:1.00, 1.67:1.00, 2.33:1.00, 3:1.00, and 4:1.00.
3. Building upon the training outcomes detailed in Section 4.2, the parameters of the improved PSO-RVM model were utilized to forecast the results. The prediction results were compared across different sample selections.

TABLE 6 Predicted results for different ratios of the training set sample amount to the testing set sample amount.

Ratio	10:30 (0.33:1.00)	15:25 (0.6:1.00)	20:20 (1:1)	22:18 (1.22:1.00)	25:15 (1.67:1.00)	28:12 (2.33:1.00)	30:10 (3:1)	32:8 (4:1)
RMSE	129.70	119.87	98.44	93.45	91.16	91.67	93.43	100.24

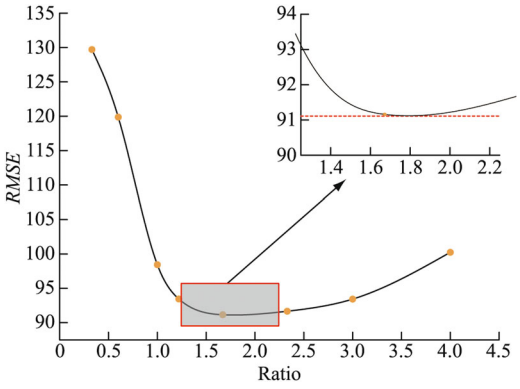

FIGURE 8 Relationship between the sample selection ratio and root mean square error (RMSE).

Table 6 and Figure 8 were generated through statistical analysis of the collected data. Table 6 presents the predicted outcomes corresponding to different ratios of the training set sample size to the testing set sample size. Notably, the *RMSE* values for ratios 1.67:1.00 and 2.33:1.00 exhibit close proximity. Figure 8 illustrates a clear downward trend in *RMSE*. Clearly observed is the decline in *RMSE* as the size of the training set increases and that of the testing set decreases. This trend shows a pronounced initial decrease followed by a more gradual decline. *RMSE* reaches its minimum and stabilizes between ratios of 1.5 and 2.0, exhibiting minimal fluctuation. As the ratio increases, *RMSE* exhibits an upward trend. This phenomenon arises due to the reduced amount of data in the testing sample group, resulting in increased result variance. Based on the aforementioned analysis, a ratio of 1.67:1.00 is recommended for sample selection in combined tests. This implies that only 62.5% of the necessary data needs to be acquired through experimentation, with the remaining 37.5% obtainable from the proposed improved PSO-RVM prediction model. The results obtained from the improved PSO-RVM model sufficiently support and supplement the data set. This approach serves as a robust machine learning tool capable of potentially replacing some true-triaxial experiments without compromising prediction accuracy.

6 | CONCLUSION

This study introduces an improved approach for the PSO algorithm and subsequently develops a RVM model based on this improved method for predicting intact rock strength. To assess the effectiveness of the proposed model, the outcomes of the improved PSO-RVM model are compared with those derived from two other machine learning models, three established PSO-improved techniques, and five empirical H–B type criteria. The training and testing of the improved PSO-RVM model utilize three datasets of true-triaxial compression strength, each covering varying ranges of the material constant m_i. To assess prediction performance, metrics including R^2, *MAPE*, *MAE*, and *RMSE* are selected for comparative evaluation.

In the three datasets, the PSO-RVM model exhibited a more balanced performance in comparison to the PSO-SVM and PSO-RF models. The proposed method of reducing inertia weights through a cubic function in this study demonstrated improved prediction accuracy and reduced computation time compared to conventional PSO-improved methods. The improved PSO-RVM model demonstrates superior performance over three-dimensional H–B type criteria across various rock types. The incorporation of hybrid kernel functions and enhancements to the PSO algorithm contribute to its high prediction accuracy and robustness. The model's outputs adhere to a Gaussian distribution, allowing for the estimation and acquisition of optimal prediction variances. Moreover, the prediction results allow for the estimation of confidence intervals, enhancing reliability. The similarity in prediction error distribution with the GZZ criterion suggests that the improved PSO-RVM model effectively captures uncertainties associated with rock characterization.

Furthermore, the proposed improved PSO-RVM model has been demonstrated as an effective machine learning tool capable of generating credible datasets. Through analysis across multiple research groups, the ratio of true-triaxial experimental data to data generated by the improved PSO-RVM model in combined tests is established at 1.67:1.00. The model's predictions are sufficiently persuasive to potentially substitute for certain true-triaxial experiments without compromising accuracy. The improved PSO-RVM model introduced in this study offers precise predictions of rock strength, providing a significant advantage over traditional true triaxial tests by reducing the time required without impeding construction progress. The model's accurate predictions facilitate informed decision-making in deep engineering projects, helping to determine supporting structures while ensuring the safety of the construction.

ACKNOWLEDGMENTS

This study is supported partially by the National Natural Science Foundation of China (42277158, 41972277, 41602300) and the State Key Laboratory of Intelligent Construction and Healthy Operation and Maintenance of Deep Underground Engineering, China University of Mining and Technology (SKLGDUEK2006).

CONFLICT OF INTEREST STATEMENT

Qi Zhang is an academic editor for *Deep Underground Science and Engineering* and was not involved in the editorial review or the decision to publish this article. The authors declare no conflict of interest.

DATA AVAILABILITY STATEMENT

The data that support the findings of this study are available from the corresponding author upon reasonable request.

REFERENCES

Azoor R, Deo R, Shannon B, Fu G, Ji J, Kodikara J. Predicting pipeline corrosion in heterogeneous soils using numerical modelling and artificial neural networks. *Acta Geotechnica*. 2022;17(4):1463-1476. doi:10.1007/s11440-021-01385-5

Babanajad SK, Gandomi AH, Alavi AH. New prediction models for concrete ultimate strength under true-triaxial stress states: an evolutionary approach. *Adv Eng Softw*. 2017;110(Aug):55-68. doi:10.1016/jadvengsoft201703011

Babanouri N, Karimi Nasab S, Sarafrazi S. A hybrid particle swarm optimization and multi-layer perceptron algorithm for bivariate fractal analysis of rock fractures roughness. *Int J Rock Mech Min Sci*. 2013;60:66-74. doi:10.1016/j.ijrmms.2012.12.028

Benz T, Schwab R. A quantitative comparison of six rock failure criteria. *Int J Rock Mech Min Sci*. 2008;45(7):1176-1186. doi:10.1016/j.ijrmms.2008.01.007

Bozorgzadeh N, Escobar MD, Harrison JP. Comprehensive statistical analysis of intact rock strength for reliability-based design. *Int J Rock Mech Min Sci*. 2018;106:374-387. doi:10.1016/j.ijrmms.2018.03.005

Ceryan N. Application of support vector machines and relevance vector machines in predicting uniaxial compressive strength of volcanic rocks. *J Afr Earth Sci*. 2014;100:634-644. doi:10.1016/j.jafrearsci.2014.08.006

Chang C, Haimson B. True triaxial strength and deformability of the German continental deep drilling program (KTB) deep hole amphibolite. *J Geophys Res: Solid Earth*. 2000;105(B8):18999-19013. doi:10.1029/2000JB900184

Contreras LF, Brown ET, Ruest M. Bayesian data analysis to quantify the uncertainty of intact rock strength. *J Rock Mech Geotech Eng*. 2018;10(1):11-31. doi:10.1016/j.jrmge.2017.07.008

Deng S, Zheng Y, Yue C, Tuan LV. Numerical investigation and analysis of intermediate principal stress effects on rock failure behaviors. *Adv Civ Eng*. 2020;2020(B10):1-11. doi:10.1155/2020/8861732

Eberhart RC, Shi Y. Comparison between genetic algorithms and particle swarm optimization. In: Proto VW, Saravanan N, Waagen D, Eiben AE, eds. *International Conference on Evolutionary Programming*. Springer; 1998:611-616.

Feng XT, Zhang X, Kong R, Wang G. A novel mogi type true triaxial testing apparatus and its use to obtain complete stress–strain curves of hard rocks. *Rock Mech Rock Eng*. 2015;49(5):1649-1662.

Gao YH, Feng XT, Zhang XW, Feng GL, Jiang Q, Qiu SL. Characteristic stress levels and brittle fracturing of hard rocks subjected to true triaxial compression with low minimum principal stress. *Rock Mech Rock Eng*. 2018;51(12):3681-3697. doi:10.1007/s00603-018-1548-4

Haimson B, Chang C. A new true triaxial cell for testing mechanical properties of rock, and its use to determine rock strength and deformability of Westerly granite. *Int J Rock Mech Min Sci*. 2000;37(1/2):285-296. doi:10.1016/S1365-1609(99)00106-9

Hoek E, Brown ET. *Underground Excavations in Rock*. CRC Press; 1980a.

Hoek E, Brown ET. Empirical strength criterion for rock masses. *J Geotech Eng Div*. 1980b;106:1013-1035.

Hoek E, Brown ET. The Hoek–Brown criterion—a 1988 update. In: Curran JH, ed. *Proceedings of the 15th Canada Rock Mechanics Symposium*. University of Toronto; 1988:31-38.

Hoek E, Brown ET. The Hoek-Brown failure criterion and GSI-2018 edition. *J Rock Mech Geotech Eng*. 2019;11(3):445-463. doi:10.1016/j.jrmge.2018.08.001

Jahed Armaghani D, Shoib RSNSBR, Faizi K, Rashid ASA. Developing a hybrid PSO–ANN model for estimating the ultimate bearing capacity of rock-socketed piles. *Neural Comput Appl*. 2015;28(2):391-405. doi:10.1002/ceat.201100437

Karimi H, McAuley KB. Bayesian estimation in stochastic differential equation models via laplace approximation. *IFAC-Pap*. 2016;49(7):1109-1114. doi:10.1016/j.ifacol.2016.07.351

Kennedy J, Eberhart RC. Particle swarm optimization. In: *Proceedings of ICNN'95-International Conference on Neural Networks*. Vol 4. IEEE; 1995:1942-1948.

Li W, Tan Z. Research on rock strength prediction based on least squares support vector machine. *Geotech Geol Eng*. 2016;35(1):385-393. doi:10.1007/s10706-016-0114-7

Liu Z, Shao J, Xu W, Wu Q. Indirect estimation of unconfined compressive strength of carbonate rocks using extreme learning machine. *Acta Geotechnica*. 2015;10:651-663. doi:10.1007/s11440-014-0316-1

Ma C, Yang J, Cheng L, Ran L. Adaptive parameter inversion analysis method of rockfill dam based on harmony search algorithm and mixed multi-output relevance vector machine. *Engineering Computations*. 2020;37(7):2229-2249. doi:10.1108/EC-09-2019-0429

Miah MI, Ahmed S, Zendehboudi S, Butt S. Machine learning approach to model rock strength: prediction and variable selection with aid of log data. *Rock Mech Rock Eng*. 2020;53(10):4691-4715. doi:10.1007/s00603-020-02184-2

Michelis P. Polyaxial yielding of granular rock. *J Eng Mech*. 1985;111(8):1049-1066. doi:10.1061/(ASCE)0733-9399(1985)111:8(1049)

Michelis P. True triaxial cyclic behavior of concrete and rock in compression. *Int J Plast*. 1987;3(3):249-270. doi:10.1016/0749-6419(87)90022-2

Miranda T, Gomes Correia A, Ribeiro e Sousa L. Bayesian methodology for updating geomechanical parameters and uncertainty quantification. *Int J Rock Mech Min Sci*. 2009;46(7):1144-1153. doi:10.1016/j.ijrmms.2009.03.008

Mogi K. Pressure dependence of rock strength and transition from brittle fracture to ductile flow. *Bull Earthq Res Inst*. 1966;44:215-232.

Mogi K. Effect of the triaxial stress system on the failure of dolomite and limestone. *Tectonophysics*. 1971a;11(2):111-127.

Mogi K. Fracture and flow of rocks under high triaxial compression. *J Geophys Res*. 1971b;76(5):1255-1269. doi:10.1029/JB076i005p01255

Mogi K. Effect of the triaxial stress system on fracture and flow of rocks. *Phys Earth Planet Inter*. 1972;5:318-324.

Pan X, Hudson JA. *A Simplified Three Dimensional Hoek–Brown Yield Criterion. Rock Mechanics and Power Plants*. Balkema; 1988.

Poli R, Kennedy J, Blackwell T. Particle swarm optimization. *Swarm Intell*. 2007;1(1):33-57. doi:10.1007/s11721-007-0002-0

Priest SD. Determination of shear strength and three-dimensional yield strength for the hoek-brown criterion. *Rock Mech Rock Eng*. 2005;38(4):299-327. doi:10.1007/s00603-005-0056-5

Ren Q, Wang G, Li M, Han S. Prediction of rock compressive strength using machine learning algorithms based on spectrum analysis of geological hammer. *Geotech Geol Eng*. 2018;37(1):475-489. doi:10.1007/s10706-018-0624-6

Shi Y, Eberhart RC. Empirical study of particle swarm optimization. In: *Proceedings of the 1999 Congress on Evolutionary Computation-CEC99 (Cat. No. 99TH8406)*. IEEE; 1999:1945-1950. doi:10.1109/CEC.1999.785511

Shinoda M, Miyata Y. PSO-based stability analysis of unreinforced and reinforced soil slopes using non-circular slip surface. *Acta Geotechnica*. 2019;14:907-919. doi:10.1007/s11440-018-0678-x

Single B, Goel RK, Mehrotra VK, Garg SK, Allu MR. Effect of intermediate principal stress on strength of anisotropic rock mass. *Tunnel Undergr Space Technol*. 1998;13(1):71-79. doi:10.1016/s0886-7798(98)00023-6

Smart BGD. A true triaxial cell for testing cylindrical rock specimens. *Int J Rock Mech Min Sci Geomech Abst*. 1995;32(3):269-275. doi:10.1016/0148-9062(94)00042-2

Song Z, Yin G, Ranjith PG, Li M, Huang J, Liu C. Influence of the intermediate principal stress on sandstone failure. *Rock Mech Rock Eng*. 2019;52(9):3033-3046. doi:10.1007/s00603-019-01756-1

Sun XM, He MC, Liu CY, et al. Development of nonlinear triaxial mechanical experiment system for soft rock specimen. *Chin J Rock Mech Eng*. 2005;24(16):2870-2874.

Takahashi M, Koide H. Effect of the intermediate principal stress on strength and deformation behavior of sedimentary rocks at the depth shallower than 2000 m. In: *ISRM International Symposium: International Society for Rock Mechanics*. OnePetro; 1989.

Tipping ME. The Relevance vector machine. In: Solla SA, Leen TK, Müller K, eds. *NIPS'99: Proceedings of the 12th International Conference on Neural Information Processing Systems*. MIT Press; 1999:652-658.

Tipping ME. Sparse Bayesian learning and relevance vector machine. *J Mach Learn Res*. 2000;1:211-244.

Tiwari RP, Rao KS. Physical modeling of a rock mass under a true triaxial stress state. *Int J Rock Mech Min Sci*. 2004;41(3):433-434. doi:10.1016/j.ijrmms.2003.12.073

Wang R, Kemeny JM. A new empirical criterion for rock under polyaxial compressive stresses. In: Daemen JJK, Schultz RA, eds. *Rock Mechanics*. Balkema; 1995:453-458.

Wang Y, Aladejare AE. Bayesian characterization of correlation between uniaxial compressive strength and Young's modulus of rock. *Int J Rock Mech Min Sci*. 2016;85:10-19. doi:10.1016/j.ijrmms.2016.02.010

Xu YH, Cai M, Zhang XW, Feng XT. Influence of end effect on rock strength in true triaxial compression test. *Can Geotech J*. 2017;54(6):862-880. doi:10.1139/cgj-2016-0393

Yagiz S, Sezer EA, Gokceoglu C. Artificial neural networks and nonlinear regression techniques to assess the influence of slake durability cycles on the prediction of uniaxial compressive strength and modulus of elasticity for carbonate rocks. *Int J Num Anal Methods Geomech*. 2012;36:1636-1650. doi:10.1002/nag.1066

Yang C, Gao W, Liu N, Song C. Low-discrepancy sequence initialized particle swarm optimization algorithm with high-order nonlinear time-varying inertia weight. *Appl Soft Comput*. 2015;29:386-394. doi:10.1016/j.asoc.2015.01.004

Yu Z, Shi X, Miao X, et al. Intelligent modeling of blast-induced rock movement prediction using dimensional analysis and optimized artificial neural network technique. *Int J Rock Mech Min Sci*. 2021;143:104794. doi:10.1016/j.ijrmms.2021.104794

Zhang L, Zhu H. Three-dimensional Hoek-Brown strength criterion for rocks. *J Geotech Geoenviron Eng*. 2007;133(9):1128-1135. doi:10.1061/(ASCE)1090-0241(2007)133:9(1128)

Zhang Q, Liu Z, Tan J. Prediction of geological conditions for a tunnel boring machine using big operational data. *Automat Constr*. 2019;100:73-83. doi:10.1016/j.autcon.2018.12.022

Zhang Q, Zhu H, Zhang L. Modification of a generalized three-dimensional Hoek–Brown strength criterion. *Int J Rock Mech Min Sci*. 2013;59:80-96. doi:10.1016/j.ijrmms.2012.12.009

Zhao J, Feng XT, Zhang X, Yang C, Zhou Y. Time-dependent behaviour and modeling of jinping marble under true triaxial compression. *Int J Rock Mech Min Sci*. 2018;110:218-230. doi:10.1016/j.ijrmms.2018.08.009

Zhao XG, Wang J, Cai M, Su GS. Influence of intermediate principal stress on the strainburst characteristics of beishan granite with consideration of end effect. *Rock Mech Rock Eng*. 2021;54(9):4771-4791. doi:10.1007/s00603-021-02526-8

AUTHOR BIOGRAPHY

Qi Zhang is a professor who works in Southeast University, China. He obtained a doctoral degree in Tongji University in 2008–2013, and studied as a visiting scholar in the Department of Civil Engineering and Mechanics at the University of Arizona for 2 years in 2009–2010 and 2012–2013. His research interests focus in three-dimensional strength criterion and constitutive model of rock mass, multi-source information fusion and evaluation of mountain tunnels, and inference of dimensionality of tunnel surrounding rock and twin modeling. He was awarded the Special Prize of the 12th Science and Technology Award by the China Society of Rock Mechanics and Engineering, as well as Future Leaders Program (2023) by ARMA. He received two doctoral thesis awards by Shanghai Municipal government and China Rock Mechanics and Engineering Society respectively. Moreover, he was appointed as the member of ASCE Rock Mechanics Committees.

How to cite this article: Zhang Q, Wang M, Wang N, Shen Y, He X. Probability prediction of true-triaxial compressive strength of intact rocks based on the improved PSO-RVM model. *Deep Undergr Sci Eng*. 2025;1-14. doi:10.1002/dug2.70007